The Role of Mitochondria, Oxidative Stress, and the Radical-binding Protein A1M in Cultured Porcine Retina.

Åkerström, Bo; CEDERLUND, MARTIN; Bergwik, Jesper; Manouchehrian, Oscar; Arnér, Karin; Holmgren Taylor, Ingrid; Ghosh, Fredrik; Taylor, Linnéa

Published in:
Current Eye Research

DOI:
10.1080/02713683.2016.1254247

2017

Document Version:
Peer reviewed version (aka post-print)

The role of mitochondria, oxidative stress and the radical-binding protein A1M in cultured porcine retina

Bo Åkerström[1], Martin Cederlund[1], Jesper Bergwik[1], Oscar Manouchehrian[2], Karin Arnér[2], Ingrid Holmgren Taylor[2], Fredrik Ghosh[2], Linnéa Taylor[2]

[1]Section for Infection Medicine, Department of Clinical Sciences, Lund University, Lund, Sweden

[2]Ophthalmology, Department of Clinical Sciences, Lund University, Lund, Sweden

Corresponding author:
Linnea Taylor
Section for Ophthalmology, Department of Clinical Sciences,
Lund University, BMC B14,
S-22184 Lund, Sweden
phone:+46 46 2220752
e-mail: linnea.taylor@med.lu.se

ABSTRACT

Purpose: The purpose of this study was to explore the relationship between oxidative stress, antioxidant defense, mitochondrial structure and biomechanical tissue support in the isolated porcine retina.

Methods: Full-thickness retinal sheets were isolated from adult porcine eyes. Retinas were cultured for 2 or 48 hours using 1) a previously established low-support explant protocol with photoreceptors positioned against the culture membrane (porous polycarbonate) or 2) a high-support procedure developed by our group, apposing the Müller cell endfeet and inner limiting membrane (ILM) against the membrane. The grafts were analyzed by quantitative PCR, immunohistochemistry, and transmission electron microscopy (TEM), and culture medium was assayed for the cell damage and oxidative stress markers lactate dehydrogenase and protein carbonyls.

Results: In explants cultured with physical support to the inner border, cone photoreceptors were preserved and lactate dehydrogenase levels were reduced, although an initial (2h), transient, increased oxidative stress was observed. Elevated expression of the antioxidants A1M (α_1-microglobulin) and heme oxygenase-1 were seen in the mitochondria-rich inner segments after 48h compared to low-support counterparts. Housekeeping gene expression suggested a higher degree of structural integrity of mitochondria in high-support explants, and TEM of inner segments confirmed preservation of a normal mitochondrial morphology.

Conclusion: Providing retinal explants with inner retinal support leads to mobilization of antioxidant proteins, preservation of mitochondrial function and increased cell viability. Consequently, the failure of low-support retinal cultures to mobilize an adequate response to

the oxidative environment may play an key role in their rapid demise. These findings shed new light on pathological reactions in biomechanically related conditions in vivo.

Keywords: α_1-microglobulin, oxidative stress, retina, mitochondria

INTRODUCTION

The delicate neuroretinal sheet is stabilized *in vivo* by a combination of physical forces. These include intraocular pressure and adhesion to retinal pigment epithelium at the outer border and the vitreous membrane at the inner border [1, 2]. Loss of of these stabilizing forces is associated with a rapid gliotic response and neuronal cell death, both in explant cultures and diseases such as retinal detachment [3, 4]. Our group has previously demonstrated that *in vitro*, these reactions can be attenuated by simulating conditions in the normal eye, either through laterally stretching retinal explants during culture, or providing the explants with physical support at the inner border [5]. This approach is believed to partially restore the collapsed network structure of the explant, and thereby curtail the Müller cell gliotic response to the trauma of the dissection procedure [6]. However, the exact mechanism behind this phenomenon remains to be explained.

Oxidative stress is a common feature observed in several retinal degenerative diseases [7-9]. For instance, oxidative stress has recently been shown to be involved in retinal degeneration during detachment *in vivo*, as well as in cell death observed in retinal explants *in vitro* [10]. Recent findings indicate that scavenging of reactive oxygen species (ROS) can attenuate retinal detachment-related photoreceptor death [11-13]. Oxidative stress refers to cell injury caused by various oxidants such as free radicals and ROS. The latter include superoxide anions, hydroxyl radicals, singlet oxygen, and hydrogen peroxide. ROS are produced by a variety of pathways of aerobic metabolism, and an important source of their production is the mitochondrial respiration [14]. Mitochondrial DNA (mtDNA) is also particularly prone to oxidative damage [15] making the mitochondria-rich retina vulnerable to oxidative damage.

Normally, ROS and other oxidants are counteracted by anti-oxidants including the high-molecular weight enzymes heme oxygenase-1 (HO-1), superoxide dismutase (SOD), catalase, and glutathione peroxidases and the low-molecular weight non-enzymatic compounds glutathione, vitamin C and E. These compounds are well-characterized, but novel antioxidants are continuously being discovered. One such molecule is the reductase, heme- and radical-binding protein A1M (α_1-microglobulin), which was shown to have protective properties against oxidative stress in cell cultures, skin and placenta [16-18], and antioxidative therapeutic effects in vivo [19-21] (reviewed in [22;23]). A1M was also recently shown to be expressed and up-regulated *in vitro* in rat retinas [10].

As mentioned above, our group has recently shown that apposing the comparatively stiff inner retina against a non-elastic culture membrane prevents the tissue collapse associated with traditional explant cultures, and provides a more permissive environment for neuronal survival in vitro [5]. For this work, we hypothesized that the differential explant survival may be due to early oxidative stress and altered mitochondrial structure. This hypothesis was tested by investigating mitochondrial morphology using transmission electron microscopy, as well as HO-1 and A1M-expression and localization in retinal explants cultured for short time periods (2h and 48h) with inner retinal support (IRS) or the standard method of placing the photoreceptors against the membrane (CO).

MATERIALS AND METHODS

Tissue Culturing

All protocols and animal treatments were in accordance with the guidelines and requirements of the government committee on animal experimentation at Lund University and with the ARVO statement on the use of animals in ophthalmic and vision research. Eyes were harvested from adult pigs aged between 4-6 months sacrificed by an overdose of sodium pentobarbital, (Apoteket, Umeå, Sweden). The neuroretinas were removed using the method described previously by Taylor et al., 2014 [6]. To summarize, the eyes were enucleated immediately after sacrifice and immersed in CO_2 –independent medium (Invitrogen, Paisley, UK). The anterior segment was excised by a sharp incision in the pars plana and cut 360 degrees. The vitreous was carefully removed in one piece using sterilized tissue paper. The neuroretinas were gently dissected free from the pigment epithelium with microforceps and the optic nerve head was cut using microscissors. Each neuroretina was sectioned into 6 pieces, each measuring approximately 6x6mm. In total, 16 eyes from 8 animals were used, yielding 74 specimens for culture, 6 specimens for baseline real time-PCR measurements (see below) and 2 eyes serving as normal adult in vivo controls. The 74 neuroretinal pieces were explanted onto Millicell-PCF 0.4 μm culture plate inserts (Millipore, Billerica, MA, USA), with either the photoreceptors (standard protocol; CO) or with the ILM positioned against the culture membrane, providing the explants with inner retinal support (IRS). Explants derived from the same eye were distributed among the culture groups to ensure no bias. Specimens were cultured in 1.5 ml DMEM/F12 (Invitrogen) supplemented with 10% fetal calf serum (Sigma-Aldrich, St Louis, MO, USA) as well as a cocktail containing 2 mM L-glutamine, 100 U/ml penicillin and 100 ng/ml streptomycin (Sigma Aldrich) for 2 hours or 2 days (48 hours). Explants originating from the same animal were divided among the groups to ensure no bias

(2h CO, n=12; 2h IRS, n=12; 2DIV CO, n=10; 2DIV IRS, n=8). The explants were maintained in an incubator at 37°C at 95% humidity and 5% CO_2. After culturing, the medium was retained for lactate dehydrogenase assay (see below).

Real time-PCR

To quantify expression of genes in retinal cells, 32 retinal explants were used (2h CO, n=6; 2h IRS, n=6; 2DIV CO, n=6; 2DIV IRS, n=6). The medium was aspirated, the tissue solubilized in 1 ml Trizol (Invitrogen, cat nr. 15596–018), and then stored at −80 °C until used for real time (RT)-PCR analysis. Messenger RNA was isolated from the Trizol-solubilized retina tissue by mixing 1 ml of the Trizol solubilized tissue with 0.2 ml chloroform, centrifuging 12,000xg 15 min, aspirating the RNA-containing upper aqueous phase, precipitating the RNA by vortexing with 0.5 ml isopropanol, and washing the pellet with 1 ml 75% ethanol. After solubilizing in H_2O, RevertAid RT Reverse Transcription Kit (Thermo Fischer Scientific) was used to transcribe mRNA to cDNA. RT-PCR was then performed using the the primers listed in Table 2. The primers were obtained from Eurofins MWG Operon and designed to hybridize to separate exons in all genes. All primer-pairs were tested in “water-controls”, i.e. complete reagent mixtures without cDNA template to ensure non-specific PCR reactions. The expression was analyzed using iQ SYBR Green Supermix (Bio-Rad). Raw data were obtained as cycle threshold values (Ct-values) and ΔCt-values were obtained by normalizing to the mean of the Ct-values of human GAPDH and β-actin. Final results are expressed as ΔΔCt-values by comparing CO- and IRS-cultures to non-cultured fresh retina samples, setting the ΔCt-values of the latter to zero for each gene.

Histology

Histological examinations were performed as previously described [24], and only briefly summarized here. After culturing, the explants were fixed in 4% paraformaldehyde in 0.1M phosphate buffer (pH 7.2) for 2h in 4 °C. The normal adult in vivo controls were fixed immediately after enucleation using the same paraformaldehyde concentration for 8h in 4 °C. The explants were infiltrated with 0.1M Sörensens medium with increasing concentrations of sucrose up to 25% for cryoprotection, after which they were embedded in egg albumin/gelatin medium for cryosectioning at -20 °C with a section thickness of 12 µm. For light microscopy, every 10th slide was stained with hematoxylin and eosin. For immunohistochemical labeling, adjoining slides with 4 sections originating from the center of the explants (the area centralis in the normal control) were chosen. The specimens were rinsed 3 times with PBS containing 0.1% Triton-X-100, and then incubated with PBS containing 0.1% Triton-X-100 and 1% bovine serum albumin (BSA) for 20 minutes at room temperature. After this, the specimens were incubated overnight at 4 °C with the respective primary antibody (Table 1). The specimens were then rinsed three times in PBS-Triton-X-100 (0.1%), and incubated for 45 minutes with a secondary fluorescein isothiocyanate (FITC) or Texas Red-conjugated antibody (Table 1) diluted in PBS-Triton-X-100 (0.1%) and 1% BSA. The specimens were then rinsed thrice in PBS-Triton-X-100 (0.1%), then mounted in Vectashield mounting medium with 4',6-diamidino-2-phenylindole (DAPI; Vector laboratories Inc., CA, USA). Negative control experiments were performed as above, replacing the primary antibody with PBS containing 0.1% Triton-X-100 and 1% BSA (see supplemental figure 1 for negative controls for all labelings). Normal porcine adult retina was used as a positive control. For each labeling, all specimens were processed in the same batch. All antibodies were titrated

through a range of working dilutions (3 orders of magnitude) to determine optimal working concentrations.

For transmission electron microscopy (TEM), cultured explants (1 from each culture group, 4 in total, as well as retina fixed immediately after enucleation) were fixed in 4% glutaraldehyde in phosphate buffer over night at 4°C. The fixation was followed by repeated rinsing in cacodylate buffer, after which the explants were post-fixed in 1% osmium tetroxide. The explants were dehydrated using increasing concentrations of ethanol, and embedded in Epon resin. Ultrathin sections (50nm) were then taken from the central part of the specimens using a Leica Ultracut UCT ultratome (Leica Microsystems, Wetzlar, Germany) equipped with a diamond knife for transmission electron microscopy.

For immunogold labeling of TEM sections, samples (1 from each culture group, 4 in total, as well as retina fixed immediately after enucleation) were fixed in 2.5 % glutaraldehyde and 2 % paraformaldehyde in 0.1 sodium cacodylic buffer (pH 7.4), for 24 h at 7° C. The samples were then transferred to 0.1 M soduim cacodylic buffer and postfixed for 2 hours in 1% osmium tetroxide solution in 0.1 M sodium cacodylic buffer. The specimens were then dehydrated in a graded ethanol series and embedded in Epon resin via acetone treatment. Ultrathin sections (50 nm) were cut using a Leica Ultracut UCT ultratome (Leica Microsystems, Wetzlar, Germany) equipped with a diamond knife. The sections were mounted on pioliform coated gold grids. Antigen retrieval was achieved by treating the samples with saturated metaperiodate for 30 minutes in room temperature. The grids were then rinsed in ddH_2O, after which they were incubated in $NaIO_4$ for 30 min. After additional rinsing in ddH_20, the grids were incubated in deactivation buffer (0.05M glycine in PBS buffer, pH 7.6) for 20 min, and then transferred to a blocking buffer (0.2% Aurion BSA in PBS buffer pH 7.6), in a humidified chamber. The specimens were then incubated over night

with the primary antibody (1:50) at 4° C in a humidified chamber. After incubation, the specimens were rinsed in 0.2% Aurion BSA in PBS buffer (pH 7.6), and then incubated with the secondary, gold-conjugated antibody (1:10) in a humidified chamber. The grids were then rinsed in 0.2% Aurion BSA in PBS buffer (pH 7.6) and 10mM phosphate buffer (pH 7.6). Finally, the grids were contrasted with 2% uranayl acetat solution, and viewed under a transmission electron microscope (see below).

Microscopy and image analysis

The histological sections and immunohistochemically labeled specimens were examined using an optical and epifluorescence microscope (Axio Imager M2, Carl Zeiss Microscopy GmbH, Jena, Germany) equipped with a digital camera system (AxioCam MRm, Carl Zeiss) and a digital acquisition system (ZEN 2012 blue edition, Carl Zeiss). When comparing immunolabeled sections, specimens were always derived from the same labeling batch, and were photographed blindly in one session using a fixed exposure time and aperture. Transmission electron microscopy specimens were examined using a 120 kV JEOL 1230 (JEOL, Herts, UK), equipped with a cooled, high-resolution digital camera (Gatan, Abingdon Oxon, UK). Images were viewed and processed using Photoshop (Adobe Systems, Mountain View, CA).

Cell viability assay

The levels of lactate dehydrogenase (LDH) in retinal explant cell culture media were measured using the CytoTox 96® Non-Radioactive Cytotoxicity Assay (Promega, Madison, WI, USA) according to the manufacturer's instructions.

Protein oxidation analysis

Protein carbonyl groups in the retinal explant cell culture media were derivatized with 2,4-dinitrophenylhydrazine according to the instructions of the OxyBlot™ Protein Oxidation Detection Kit (https://www.merckmillipore.com/SE/en/product/OxyBlot-Protein-Oxidation-Detection-Kit, MM_NF-S7150?bd=1#anchor_PI). SDS-PAGE of 1 µl derivatized medium (appr. 8 µg protein) was performed with pre-cast 4-20 % gels bought from Bio-Rad **(Mini-PROTEAN Tris-Glycine, Stain-Free, 4-20%)**. The proteins were transferred to PVDF membranes by electroblotting (Transblot® Turbo, Bio-Rad), the membranes incubated with the supplied antibodies from the OxyBlot™ kit according to the manufacturer's instructions, and developed using Clarity™ Western ECL Substrate (Bio-Rad). **Reading and digitalization** of the **blotting intensity on the** membranes was performed using a ChemiDoc™ MP System (Bio-Rad), and density analysis was done using Image Lab™ Software (Bio-Rad).

Statistical Analysis

Data from RtPCR, LDH and DNA oxidation analysis were analyzed using One-Way ANOVA with a Bonferroni post-hoc test (Originlab; OriginPro 8 Software, Northamton, MA). For Values of $p<0.05$ were considered significant.

Immunohistochemically labeled sections were used to statistically quantify the expression of HO-1, **vimentin** and A1m, and for cell counts of transducin-labeled photoreceptor cell bodies and NeuN-labeled ganglion cells. The cell counts and labeling intensity measurements and were performed in a blinded manner, using a method previously described by Manouchehrian et al. in 2015 [38]. In summary, three central sections per explant were analyzed for each labeling, with three sections per normal adult in vivo control. The in vivo controls and cultured specimens were processed in the same batch, with the same imaging

settings, for each labeling. From each section, three images were taken, and the mean fluorescence intensity was measured or labeled cell counted at 20x magnification. For transducin labeling, cells located in the outer ONL were counted. For NeuN labeling, only large cells of a ganglion morphology located in the GCL were counted. The images taken for fluorescence intensity measurements were analyzed using ImageJ (Rasband, W.S., ImageJ, U. S. National Institutes of 306 Health, Bethesda, MD, http://imagej.nih.gov/ij/), as previously described [38]. A rectangular area of 770x750 pixels was analyzed, placed so that the area of interest included the entire inner-to-outer retinal areas, except the culture membrane, to exclude contribution from autofluorescence. The channels were separated, the background subtracted, and the mean fluorescence value was noted for each image. A representative picture was chosen from each labeling batch for image compilation. Raw data from the cell counts and intensity measurements was used to generate mean values for the various groups, and analyzed using a one-way ANOVA with a Tukey post hoc test (GraphPad InStat; GraphPad Software, San Diego, CA). Values of $p<0.05$ were considered significant.

RESULTS

Immunohistochemistry

A1M: Staining of normal adult porcine retina with anti-A1M revealed strong labeling of A1M deposition in structures at the innermost border of the retina (Fig. 1A). CO specimens cultured for 2h displayed similar labeling of structures at the innermost border of the specimen (Fig. 1B). Corresponding IRS explants showed high intensity labeling of structures in the innermost retina, as well as weak labeling of photoreceptor inner segments (Fig. 1C). After 48h, CO specimens showed only weak labeling of scattered structures at the inner and outer borders of the explant, as well as of isolated structures in the inner nuclear layer (INL), inner plexiform layer (IPL) and inner segments (Fig. 1D). In contrast, IRS specimens cultured for 48h revealed general labeling throughout the explant, as well as strong labeling of scattered structures present in the inner layers and the outer plexiform layer (OPL), and high intensity labeling of inner segments (Fig. 1E). Fluorescence intensity measurements revealed significantly stronger labeling intensity present in 2h IRS specimens compared to corresponding CO explants (**$p<0.001$;** Fig. 1F). After 48h, both groups displayed high labeling intensity, with no difference between the groups.

HO-1 and Vimentin: Normal adult porcine retina displayed HO-1 labeling in Müller cell endfeet at the innermost border of the specimen and structures in the ONL, as well as weak labeling of the IPL and OPL (Fig. 2A). Anti-vimentin staining showed strong labeling of Müller cell endfeet and weak labeling of Müller cell fibers vertically spanning the specimen from inner to outer border. After 2h, CO explants showed scattered HO-1 labeling in photoreceptor inner segments with weak labeling of structures in the outer ONL, in a pattern corresponding to cone photoreceptors and their terminals (Fig. 2B). Vimentin labeling was observed in the Müller cell endfeet and in occasional fibers in the IPL and INL. IRS

specimens cultured for 2h showed HO-1 labeling of photoreceptor inner segments and weak labeling of structures in the ONL (Fig. 2C). Vimentin labeling was seen in Müller cell endfeet, and in weakly labeled fibers spanning the retinal layers from inner to outer border. After 48h, CO specimens displayed HO-1 labeling of structures at the inner and outer border of the explant (Fig. 2D). Vimentin labeling was found in thick, slightly disorganized vertical fibers spanning the explant from inner to outer border, with strong labeling in the Müller cell endfeet. IRS explants cultured for 48h showed strong HO-1 labeling in Müller cell endfeet at the innermost border, as well as in unidentifiable structures in the IPL and ONL, and in inner segments (Fig. 2E). Vimentin labeling was present in Müller cell endfeet and in fibers spanning the retinal layers. Fluorescence intensity measurements revealed a slight downregulation of HO-1 expression in both explants types at 2h, with no significant difference between the groups (Fig. 2F). After 48h, IRS specimens revealed a significant upregulation of HO-1 expression compared to CO counterparts, which remained below baseline ($p<0.001$). **No significant difference in vimentin fluorescence intensity was observed between the groups (statistical data not shown).**

GFAP: GFAP labeling of normal adult pig retina revealed strong labeling of Müller cell endfeet and astrocytes at the inner border, with very weak labeling of thin Müller cell fibers vertically spanning the retinal layers, which is normal for this species (Fig. 3A). 2h IRS and CO explants displayed labeling similar to that observed in the normal control (Fig. 3B-C). After 48h, CO explants revealed labeling of slightly hypertrophic and disorganized Müller cell fiber spanning the retina from inner to outer border (Fig. 3D). In contrast, corresponding IRS specimens revealed a labeling pattern similar to 2h counterparts (Fig. 3E). Fluorescence intensity measurements revealed no significant difference in GFAP expression between the

explant groups at 2h, however, at 48h, CO explants revealed a significant upregulation compared to IRS counterparts ($p<0.001$; Fig. 3F).

Transducin: Transducin labeling of normal adult porcine retina showed cone photoreceptor cell bodies in the outer part of the outer nuclear layer (ONL), as well cone inner segments and terminals in the OPL (Fig. 4A). Strong labeling was also present in bipolar cell perikarya located in the IN, and in their processes vertically spanning the INL and terminating in the innermost IPL. After 2h in vitro, CO specimens displayed strong labeling of cone cell bodies in the outer ONL, their inner segments as well as in their terminals in the OPL (Fig. 4B). Compared with the normal control, slightly fewer bipolar cell bodies were labeled in the INL, and the labeling of their vertical processes in the inner layers appeared weaker and more condensed. In contrast, 2h IRS specimens displayed labeling of cone cell bodies in the outer ONL as well as in the inner segments and terminals in the OPL (Fig. 4C). Only very weak labeling was present in bipolar cell perikarya and processes. After 48h in culture, CO explants showed strong labeling in disorganized cone cell bodies in the outer ONL as well as in inner segment debris and in the cone terminals (Fig. 4D). Weak labeling of bipolar cell processes was present in the IPL. 48h IRS specimens revealed labeling of cone cell bodies in the outer ONL as well as in inner segments and terminals in the OPL (Fig. 4E). The number of labeled cell bodies in the ONL was significantly higher in IRS specimens compared to corresponding CO explants ($p>0.001$; Fig. 4F).

NeuN: Large NeuN-labeled cells of ganglion morphology were present in the ganglion cell layer (GCL) in the normal adult pig retina (Fig. 5A). CO explants at both time points revealed a significant reduction in the number of labeled cells present in the GCL compared to corresponding IRS specimens ($p<0.001$; Fig. 5B-F).

Transmission electron microscopy

Transmission electron microscopy of normal adult porcine retina revealed inner segments densely populated with dark mitochondria with a normal morphology (Fig. 6A-B). CO explants displayed a multitude of inner segments with less electron-dense mitochondria with few cristae (Fig. 6C). Corresponding IRS specimens cultured for 2h displayed inner segments with dark, albeit slightly swollen mitochondria, as well as the occasional disrupted inner segment (Fig. 6D). After 48 h, CO explants displayed few intact inner segments, and the remaining mitochondria displayed a distended, rounded morphology with membrane disruption evident (Fig. 6E). In contrast 48 h, IRS specimens displayed slightly truncated inner segments densely populated with dark mitochondria (Fig. 6F).

A1M-immunogold labeling was performed to visualize A1M presence in various cellular compartments. Sections of normal adult porcine retina revealed labeling mainly in inner segment mitochondria, with large clusters of labeling present (Fig. 7A). Smaller clusters of labeling were also present in cell nuclei in the ONL (Fig. 7B). In 2h CO explants, scattered large clusters of labeling were present in distended inner segment mitochondria (Fig. 7C). Only isolated labeling was observed in cell nuclei in the ONL (not shown). Similar labeling was found in 2h IRS specimens, although the labeling appeared concentrated to the outer mitochondrial membrane (Fig. 7D). In 48h CO explants, large, rounded inner segment mitochondria displayed scattered labeling (Fig. 7E). 48h IRS specimens displayed scattered labeling present throughout the inner segment mitochondria (Fig. 7F).

Cell viability and protein oxidation markers

Significantly higher levels of protein carbonyl groups were seen after 2h in IRS cultured retinas compared to CO-cultures (Fig. 8A and B, $p<0.001$). After 48 h, less protein carbonyls were seen and the amounts did not differ between IRS and CO-cultures. Thus, the results

suggest a transient oxidative stress peak after 2 h in the IRS-cultures. The interpretation of these results are based on the hypothesis that oxidative stress-induced carbonylation is non-specific, i.e. that protein carbonyl groups are formed on all proteins regardless of the identities of the proteins. This is supported by the results in Fig 8A-B since, according to this hypothesis, a similar variation in blotting intensities of the samples should be seen whether the total optical densities of the separate bands, or the total optical density of the whole lanes were measured (Fig 8B). **Hence, the carbonylated protein bands in the medium were not investigated, but are most likely components of fetal calf serum, a component of the culture medium**. A significantly higher leakage of the cell viability marker LDH to the culture medium could be seen in CO retinas compared to IRS cultured retina after 48h (Fig. 6B, $p<0.05$), whereas no significant difference was seen after 2h of incubation.

RT-PCR

The mRNA expression of the genes coding for A1M and HO-1 (antioxidation genes), S12 (mitochondrial housekeeping gene), and p21 (cell cycle arrest marker) was measured by RT-PCR in CO and IRS porcine retinas after 2h and 48h (Fig. 9). S12 mRNA, which may be used as a marker of mitochondrial density in the samples at each time-point and culturing condition, was significantly higher in IRS-cultures after 2 h ($p<0.001$), and HO-1 and S12 mRNA were significantly elevated in IRS retinas compared to CO retinas after 48h ($p<0.01$ and $p<0.001$, respectively). The results thus suggest an up-regulation of the antioxidation gene HO-1 in IRS cultures after 48h, and a higher density of mitochondria in IRS cultures compared to CO cultures at both time-points.

DISCUSSION

Perspective

In this study, we have explored mechanisms involved in retinal homeostasis in two culture settings, the traditional low-support model, and our own system providing explants with support at the inner border. We have previously described that introducing biomimetic stretch and inner retinal support to adult retinal explants significantly extends survival time *in vitro,* and that the standard culturing procedure without mechanical support induces degenerative changes as early as after 3h in vitro [5, 6; 39]. Here, we have addressed the influence of oxidative stress, antioxidation defense and mitochondrial function in the above described settings. The results show that providing the explants with physical support at the inner border leads to an increased cell viability, and allows upregulation of antioxidant protein expression and maintenance of mitochondrial morphology in the photoreceptor inner segments. These findings suggest that retinas cultured with inner support (IRS) obtain a prolonged survival partly by up-regulating the expression of antioxidants.

Oxidative stress, antioxidants and endogenous defenses in the cultured retina

Oxidative stress is involved in many retinal diseases [9] and elevated levels of protein carbonyl groups are widely used as a biomarker for oxidative stress [25]. Increased formation of protein carbonyls was seen in IRS cultures after 2 h (Fig 8), as compared to CO-cultures, suggesting an early peak of oxidative stress in IRS culture conditions. However, a lower degree of cell death, measured by LDH concentration in the culture medium was seen in the IRS cultures as compared to CO cultures after 48h (Fig. 8). **The increased mRNA expression of HO-1 in IRS cultured retinas suggests that they have an increased capacity** to mount defensive mechanisms against oxidative stress (Fig. 9). **This may be a result of the**

initial transient oxidative stress formation in the IRS cultures, shown in Fig 8A-B. No increase of A1M mRNA expression was seen in the IRS cultures, despite of the significantly stronger staining of the IRS specimen with anti-A1M after 2h. This may be explained by an increased uptake of extracellular A1M originating from blood plasma. Uptake of extracellular A1M has previously been shown to be an important mechanism of damaged cells to strengthen its antioxidation defence [16,26]. Thus, it may be speculated that the early, transient oxidative stress in the IRS cultures induces an increased uptake of A1M to reinforce the antioxidation defence. Furthermore, A1M and HO-1 proteins were mainly localized to the photoreceptor inner segments (Fig. 1 and 2), the region which also showed the most striking difference in mitochondrial morphology (Fig. 4; see next paragraph for further discussion). Deposition of A1M was also present at the innermost retinal border, an area rich in proteins regulating biochemical homeostasis, such as glutamine synthetase, carbonic anhydrase and CRALBP, where A1M may have waste-product clearance functions as previously described in other organ systems [22].

The role of mitochondria

The high oxygen consumption of the photoreceptors is well known. To provide the photoreceptors with sufficient energy the inner segments are densely populated by mitochondria and the cell survival is highly dependent on their intact function. In this work, we show that IRS culture conditions are associated with maintenance of mitochondrial morphology in the photoreceptor inner segments. Furthermore, a higher mitochondria density in IRS specimens is indicated by immunohistochemistry, TEM, **as well as an increased mRNA expression of S12, a mitochondrial housekeeping gene in the IRS specimen.** Interestingly, our results show expression of A1M and HO-1 in this area (Fig.1,2), and an enhanced expression in IRS specimens. A1M was also seen localized to mitochondrial

membranes using transmission electron microscopy and immunogold labeling (Fig. 5). A1M is known to have protective effects against oxidative stress [22]. It has recently been shown that A1M binds to the membranes of mitochondria in apoptotic cells, which results in the maintenance of an intact morphological structure and ATP-production of the mitochondria under conditions of oxidative stress [26]. Mitochondrial alterations, such as permeability transition (PT), are known to constitute critical events of the apoptotic cascade [27], and the apoptosis-associated changes in cellular redox potentials (hypergeneration of superoxide anion, oxidation of compounds of the mitochondrial membrane) may be inhibited by A1M bound to the mitochondrial membrane.

The role of Müller cells

One possible mechanism behind the increased capability of IRS-cultured explants to counteract oxidative stress and increase survival compared to standard cultured specimens may be found in the Müller cells, whose normal functions include maintaining the biochemical homeostasis of the tissue [29]. It has also been suggested that these cells are able to regulate the biomechanical properties of the retina through changes in the expression of cytoskeletal intermediary filaments, such as GFAP and vimentin [28-30]. Müller cells have been found to express mechanosensory Ca^{2+} ion channels [2, 31-33] which respond to changes in cell membrane tensility by Ca^{2+} influx [31,35]. The influx of Ca^{2+} can in turn cause an upregulation of intermediary filaments, thereby stiffening the tissue, an event associated with reactive gliosis [29, 30, 33-36]. Previous studies by our group, confirmed by the results presented herein, show that this occurrence is relatively late, with significant upregulation of GFAP present only after 48h [39]. Reactive gliosis is the response to virtually all forms of pathological changes in the retina, and is associated with a loss of the normal Müller cell homeostatic functions, such as maintaining water and ion balance and

neurotransmitter recycling through glutamine synthetase, leading to a neurotoxic environment [29]. This process is observed during various forms of injury and disease [6, 29, 30, 37]. The loss of metabolic functions further include supplying the neurons with nutrients. Deprivation of essential nutrition could explain the inability to mount a sufficient defense against the oxidative, apoptotic milieu initiated by the removal of the retina from the normal environment of the eye, including the axotomy of the ganglion cells. This may lead to a downward spiral where the mitochondria, sensitive to oxidative stress, lose their function, which increases apoptosis through the release of caspases. This degenerative damage can further exacerbate glial reactivity, which can lead to total collapse [6, 29]. Thus, in our low-support CO explants, the tissue collapse associated with the explant procedure, coupled with increased oxidative stress, may cause reactive changes in the Müller cells which exceed their capacity overcome, leading to further degenerative damage, seen in the loss of cone photoreceptors (transducin) and ganglion cells (NeuN). However, if this initial onslaught can be inhibited the survival may be enhanced not only in vitro but also in vivo, for example in the case of retinal detachment.

Conclusion

In this study, we have shown that providing retinal explants with physical support to the inner border results in an early attenuation of degenerative damage and an increased capacity to cope with oxidative stress through the endogenous upregulation of HO-1 and A1M. This indicates the importance of biomechanical forces for retinal homeostasis, and increases our understanding of pathological reactions observed in retinal diseases with biomechanical components.

FUNDING

This project was funded by grants from the Lund University Faculty of Medicine, University of Lund, Region Skåne (ALF), The Swedish Research Council, The Princess Margaretas Foundation for Blind Children, The Swedish Eye Foundation, Österlunds Foundation, and A1M Pharma AB.

DECLARATION OF INTERESTS

None of the authors has any conflicting interests to disclose. BÅ is a co-founder and share-holder of the company A1M Pharma AB, which has funded parts of this study. A1M Pharma, however, has no role in design, data collection and analysis, decision to publish, or preparation of the manuscript.

ACKNOWLEDGEMENTS

The authors are grateful for the excellent technical and infrastructural help of Maria E Johansson, Lina Gefors and Ola Gustafsson.

TABLE 1. Primary and secondary antibodies used for immunohistochemical analysis.

ANTIGEN	TARGET	SPECIES	DILUTION	SOURCE
Urine A1M (α_1-microglobulin)	A1M	Mouse MAb	10 µg/ml	23.26; in-house production
HO-1 (heme oxygenase)	HO-1	Rabbit polyclonal	1:100	Bioss, Woburn, MA, USA
Transducin Gβ3 (C-16)	Cone photoreceptors, cone bipolar cells	Mouse polyclonal	1:500	Santa Cruz Biotech Inc, Dallas TX, USA
Vimentin	Müller cells	Mouse MAb	1:500	Chemicon Int., Temecula, CA, USA
GFAP	Astrocytes, Müller cells	Mouse MAb	1:500	Chemicon Int., Temecula, CA, USA
SECONDARY ANTIBODY	**TARGET**	**SPECIES**	**DILUTION**	**SOURCE**
FITC-conjugated anti-mouse IgG	Mouse IgG	Goat polyclonal	1:200	Sigma Aldrich, St Louis, MO, USA
Rhodamine Red TM -X-conjugated	Rabbit IgG	Donkey polyclonal	1:200	Jackson ImmunoResearch, PA, USA
5 nm gold-conjugated anti-mouse IgG	Mouse IgG	Goat	1:10	Ted Pella Inc., Redding, CA, USA

TABLE 2. PRIMERS used for RT-PCR analysis.

Protein	Forward	Reverse
A1M	ACATTGCCCAATGACATC	TCACCTCACAGATACCTT
HO-1 (heme oxygenase)	CTGGAGGAGGAGATTGAGC	TTGGCGACATTGGGGAAAG
GAPDH	CCACCCATGGCAAATTCCATGGCA	TCTAGACGGCAGGTCAGGTCCACC
β-actin	CCACGAAACTACCTTCAACTCC	GTGATCTCCTTCTGCATCCTGT
S12	AAAGGACTTGGCGGTGCTT	GTTACGACTTGTCTCTTCGTGCA
p21	CTTGGTCTGCCCAAGATCTAC	AACAGGTCCACATGGTCCTC

REFERENCES

1. Marmor MF, Yao XY, Hageman GS. Retinal adhesiveness in surgically enucleated human eyes. Retina 1994;14(2):181-186.

2. Franze K, Francke M, Gunter K, Christ AF, Korber N, Reichenbach A et al. Spatial mapping of the mechanical properties of the living retina using scanning force microscopy. Soft Matter 2011;7(7):3147-3154.

3. Lewis GP, Matsumoto B, Fisher SK. Changes in the organization and expression of cytoskeletal proteins during retinal degeneration induced by retinal detachment. Investigative ophthalmology & visual science 1995;36(12):2404-2416.

4. Winkler J, Hagelstein S, Rohde M, Laqua H. Cellular and cytoskeletal dynamics within organ cultures of porcine neuroretina. Exp Eye Res 2002;74(6):777-788.

5. Taylor L, Moran D, Arner K, Warrant E, Ghosh F. Stretch to See: Lateral Tension Strongly Determines Cell Survival in Long-Term Cultures of Adult Porcine Retina. Investigative ophthalmology & visual science 2013;54(3):1845-1856.

6. Taylor L, Arner K, Taylor IH, Ghosh F. Feet on the Ground: Physical Support of the Inner Retina Is a Strong Determinant for Cell Survival and Structural Preservation In Vitro. Investigative ophthalmology & visual science 2014;55(4):2200-2213.

7. Beatty S, Koh HH, Henson D, Boulton M. The role of oxidative stress in the pathogenesis of age-related macular degeneration. Surv Ophthalmol 2000;45(2):115-134.

8. Winkler BS, Boulton ME, Gottsch JD, Sternberg P. Oxidative damage and age-related macular degeneration. Mol Vis 1999;5(24-35).

9. Oduntan OA, Mashige KP. A review of the role of oxidative stress in the

pathogenesis of eye diseases. S Afr Optom 2011;70(4):191-199.

10. Cederlund M, Ghosh F, Arnér K, Andreasson S, Åkerström B. Vitreous levels of oxidative stress biomarkers and the radical-scavenger alpha-1-microglobulin/A1M in human rhegmatogenous retinal detachment. Graefe's Arch Clin Exp Ophthalmol 2013;251(3):725-732.

11. Roh MI, Murakami Y, Thanos A, Vavvas DG, Miller JW. Edaravone, an ROS scavenger, ameliorates photoreceptor cell death after experimental retinal detachment. Invest Ophthalmol Vis Sci 2011;52(6):3825-3831.

12. Mantopoulos D, Murakami Y, Comander J, Thanos A, Roh M, Miller JW et al. Tauroursodeoxycholic acid (TUDCA) protects photoreceptors from cell death after experimental retinal detachment. PloS One 2011;6(9):e24245.

13. Trichonas G, Murakami Y, Thanos A, Morizane Y, Kayama M, Debouck CM et al. Receptor interacting protein kinases mediate retinal detachment-induced photoreceptor necrosis and compensate for inhibition of apoptosis. Proc Nat Acad Sci U.S.A. 2010;107(50):21695-21700.

14. Poyton RO, Ball KA, Castello PR. Mitochondrial generation of free radicals and hypoxic signaling. Trends Endocrinol Metab 2009;20(7):332-340.

15. Liang FQ, Godley BF. Oxidative stress-induced mitochondrial DNA damage in human retinal pigment epithelial cells: a possible mechanism for RPE aging and age-related macular degeneration. Exp Eye Res 2003;76(4):397-403.

16. Olsson MG, Olofsson T, Tapper H, Åkerström B. The lipocalin alpha-1-microglobulin protects erythroid K562 cells against oxidative damage induced by heme and reactive oxygen species. Free Radic Res 2008;42(8):725-736.

17. Olsson MG, Allhorn M, Larsson J, Cederlund M, Lundqvist K, Schmidtchen A et al. Up-regulation of A1M/alpha-1-microglobulin in skin by heme and reactive oxygen species gives protection from oxidative damage. PloS One 2011;6(11):e27505.

18. May K, Rosenlöf L, Olsson MG, Centlow M, Mörgelin M, Larsson I et al. Perfusion of human placenta with hemoglobin introduces preeclampsia-like injuries that are prevented by alpha-1-microglobulin. Placenta 2011;32(4):323-332.

19. Wester-Rosenlöf L, Casslén V, Axelsson J, Edström-Hägerwall A, Gram M, Holmqvist M et al. A1M/alpha-1-microglobulin protects from heme-induced placental and renal damage in a pregnant sheep model of preeclampsia. PloS One 2014;9(1):e86353.

20. Sverrisson K, Axelsson J, Rippe A, Gram M, Åkerström B, Hansson SR et al. Extracellular fetal hemoglobin induces increases in glomerular permeability: inhibition with alpha1-microglobulin and tempol. Am J Physiol Renal Physiol 2014;306(4):F442-448.

21. Nääv A, Erlandsson L, Axelsson J, Larsson I, Johansson M, Wester-Rosenlöf L et al. A1M ameliorates preeclampsia-like symptoms in placenta and kidney induced by cell-free fetal hemoglobin in rabbit. PloS One 2015;10(5):e0125499.

22. Åkerström B, Gram M. A1M, an extravascular tissue cleaning and housekeeping protein. Free Rad Biol Med 2014:74:274-282.

23. Olsson MG, Allhorn M, Bülow L, Hansson SR, Ley D, Olsson ML et al. Pathological conditions involving extracellular hemoglobin: molecular mechanisms, clinical significance, and novel therapeutic opportunities for alpha-1-microglobulin. Antiox Redox Signal 2012;17(5):813-846.

24. Engelsberg K, Ghosh F. Transplantation of cultured adult porcine full-thickness retina. Cell transplant 2007;16(1):31-39.

25. Buss H, Chan TP, Sluis KB, Domigan NM, Winterbourn CC. Protein carbonyl measurement by a sensitive ELISA Method. Free Radic Biol Med 1997;23(3):361-366.

26. Olsson MG, Rosenlöf LW, Kotarsky H, Olofsson T, Leanderson T, Mörgelin M et al. The radical-binding lipocalin A1M binds to a Complex I subunit and protects mitochondrial structure and function. Antiox Redox Signal 2013;18(16):2017-2028.

27. Hirsch T, Marchetti P, Susin SA, Dallaporta B, Zamzami N, Marzo I et al. The apoptosis-necrosis paradox. Apoptogenic proteases activated after mitochondrial permeability transition determine the mode of cell death. Oncogene 1997;15(13):1573-1581.

28. Lindqvist N, Liu Q, Zajadacz J, Franze K, Reichenbach A. Retinal glial (Müller) cells: Sensing and responding to tissue stretch. Invest Ophthalmol Vis Sci 2010;51(3):1683-1690.

29. Bringmann A, Pannicke T, Grosche J, Francke M, Wiedemann P, Skatchkov SN et al. Müller cells in the healthy and diseased retina. Prog Retin Eye Res 2006;25(4):397-424.

30. Bringmann A, Iandiev I, Pannicke T, Wurm A, Hollborn M, Wiedemann P et al. Cellular signaling and factors involved in Muller cell gliosis: neuroprotective and detrimental effects. Prog Retin Eye Res 2009;28(6):423-451.

31. Ryskamp DA, Witkovsky P, Barabas P, Huang W, Koehler C, Akimov NP et al. The polymodal ion channel transient receptor potential vanilloid 4 modulates calcium flux, spiking rate, and apoptosis of mouse retinal ganglion cells. J Neurosci 2011;31(19):7089-7101.

32. Lu YB, Franze K, Seifert G, Steinhäuser C, Kirchhoff F, Wolburg H et al. Viscoelastic properties of individual glial cells and neurons in the CNS. Proc Natl Acad Sci U.S.A. 2006;103(47):17759-17764.

33. Lu YB, Iandiev I, Hollborn M, Korber N, Ulbricht E, Hirrlinger PG et al. Reactive glial cells: increased stiffness correlates with increased intermediate filament expression. FASEB J 2011;25(2):624-631.

34. Lewis GP, Erickson PA, Guerin CJ, Anderson DH, Fisher SK. Basic fibroblast growth factor: a potential regulator of proliferation and intermediate filament expression in the retina. J Neurosci 1992;12(10):3968-3978.

35. Phan MN, Leddy HA, Votta BJ, Kumar S, Levy DS, Lipshutz DB, et al. Functional Characterization of TRPV4 as an Osmotically Sensitive Ion Channel in Porcine Articular Chondrocytes. Arthritis Rheum 2009;60(10):3028-3037.

36. Loukin S, Zhou XL, Su ZW, Saimi Y, Kung C. Wild-type and Brachyolmia-causing Mutant TRPV4 Channels Respond Directly to Stretch Force. J Biol Chem 2010;285(35):27176-27181.

37. Hauck SM, Suppmann S, Ueffing M. Proteomic profiling of primary retinal Muller glia cells reveals a shift in expression patterns upon adaptation to in vitro conditions. Glia 2003;44(3):251-263.

38. Manouchehrian O, Arnér K, Deierborg T, Taylor L. Who let the dogs out?: detrimental role of Galectin-3 in hypoperfusion-induced retinal degeneration. J Neuroinflammation. 2015;12:92.

39. Ghosh F, Arnér K, Taylor L. In vitro biomechanical modulation-retinal detachment in a box. Graefes Arch Clin Exp Ophthalmol. 2016;254(3):475-87.

FIGURE LEGENDS

Figure 1: Immunohistochemical labeling of A1M. A) Normal porcine retina. B) 2h CO-cultured retina. C) 2h IRS-cultured retina. D) 48h CO-cultured retina. E) 48h IRS cultured retina. F) Statistical analysis of A1M labeling intensity. $p<0.001$ = ***. Abbreviations: GCL= ganglion cell layer, IPL = inner plexiform layer, INL = inner nuclear layer, ONL = outer nuclear layer, IS = photoreceptor inner segments. Scale bar = 50µm. The bars show mean±SEM.

Figure 2: Immunohistochemical double labeling of heme oxygenase 1 (HO-1; red) and vimentin (green) and DAPI (blue). A) Normal porcine retina. B) 2h CO-cultured retina. C) 2h IRS-cultured retina. D) 48h CO-cultured retina. E) 48h IRS cultured retina. F) Statistical analysis of HO-1 labeling intensity. $p<0.001$ = ***. Abbreviations: GCL= ganglion cell layer, IPL = inner plexiform layer, INL = inner nuclear layer, ONL = outer nuclear layer, IS = photoreceptor inner segments. Scale bar = 50µm. The bars show mean±SEM.

Figure 3: Immunohistochemical labeling of astrocytes and activated Müller cells with GFAP. A) Normal porcine retina. B) 2h CO-cultured retina. C) 2h IRS-cultured retina. D) 48h CO-cultured retina. E) 48h IRS cultured retina. F) Statistical analysis of GFAP labeling intensity. $p<0.001$ = ***. Abbreviations: GCL= ganglion cell layer, IPL = inner plexiform layer, INL = inner nuclear layer, ONL = outer nuclear layer, IS = photoreceptor inner segments. Scale bar = 50µm. The bars show mean±SEM.

Figure 4: Immunohistochemical labeling of cone photoreceptors and bipolar cells with transducin. A) Normal porcine retina. B) 2h CO-cultured retina. C) 2h IRS-cultured retina. D) 48h CO-cultured retina. E) 48h IRS cultured retina. F) Statistical analysis of transducin-labeled cell bodies. $p<0.001$ = ***. Abbreviations: GCL=

ganglion cell layer, IPL = inner plexiform layer, INL = inner nuclear layer, ONL = outer nuclear layer, IS = photoreceptor inner segments. Scale bar = 50µm. Error bars SEM.

Figure 5: Immunohistochemical labeling of ganglion cells in the GCL with NeuN. A) Normal porcine retina. B) 2h CO-cultured retina. C) 2h IRS-cultured retina. D) 48h CO-cultured retina. E) 48h IRS cultured retina. F) Statistical analysis of NeuN-labeled cell bodies. $p<0.001$ = ***. Abbreviations: GCL= ganglion cell layer. Scale bar = 50µm. The bars show mean±SEM.

Figure 6: Transmission electron microscopy of inner segment in adult porcine retina. Normal adult porcine retina (A-B), 2h CT explants (C), 2h IRS explants (D) 48h CT explants (E), 48h IRS explants (E). A) Transmission electron microscopy of normal adult porcine retina reveals inner segments (IS) distal to the outer limiting membrane (OLM) and the outer nuclear layer, which is populated with numerous photoreceptor nuclei (Ph). Scale bar = 5µm. **B)** IS densely populated with dark mitochondria with a normal morphology. Scale bar = 1µm. **C)** CT explants cultured for 2 h show a multitude of inner segments with pale, disrupted mitochondria. Scale bar = 1µm.**D)** IRS specimens cultured for 2h display IS with morphologically normal mitochondria, as well as IS containing dark, slightly swollen mitochondria. The occasional disrupted IS can be seen. Scale bar = 2µm. **E)** In contrast, 48 h CT explants display few intact inner segments, and the mitochondria found show a distended, round morphology with membrane disruption. Scale bar = 0.5µm **F)** After 48 h, IRS specimens reveal slightly truncated inner segments densely populated with dark mitochondria. Scale bar = 5µm.

Figure 7: Transmission electron microscopy of immunogold-labeled A1M (arrows) in normal adult porcine retina and cultured retinal explants. Normal adult porcine retina (A-B), 2h CT explants (C), 2h IRS explants (D) 48h CT explants (E), 48h IRS explants

(E). A). Inner segment mitochondria with immunogold-labeled A1M. Scale bar = 2µm. **B)** Photoreceptor nuclei with immunogold labeled A1M. Scale bar = 1µm. **C)** Distended inner segment mitochondria with scattered immunogold-labeled A1M. Scale bar = 0,5µm. **D)** Immunogold-labeled A1M located in the outer mitochondrial membrane of an inner segment mitochondrion. Scale bar = 0.2µm. **E)** Distended inner segment mitochondria with labeled A1M. Scale bar = 0.5µm **F)** Scattered labeling present throughout the inner segment mitochondria. Scale bar = 0.2µm.

Figure 8: A) Detection of protein carbonylation in the media of CO- and IRS-cultured porcine retinas after 2h and 48h using Western blotting-based **OxyBlot™ Protein Oxidation Detection Kit. 0.1 ml medium was used for the carbonyl group analyses. B) Digitalized optical densities of bands 1 and 4, and the whole lanes, shown in panel A. Each column represents mean±SEM (n=6). The optical density means of the CO-cultures at 2h were set to 1.0.** C) Cell viability measured by leakage of LDH to the medium from CO- and IRS-cultured porcine retinas after 2h and 48 h. The medium was diluted 10x before measurement. The bars show mean±SEM, n=6). *=p<0,05; ***=p<0.001.

Figure 9: Expression levels of HO-1, S12, p21 and A1M genes measured by RT-PCR. Ct-values were re-calculated to ΔCt-values by normalizing to the average of Ct-values of human glyceraldehyde-3-phosphate dehydrogenase (GAPDH) and β-actin. The ΔΔCt-values shown in the figure were then calculated by normalizing 2h and 48h cultured retinas against non-cultured retina specimens. Hence, the bars show the relative increase/decrease of gene expression in (IRS) after 2h and 48h as compared to fresh, non-cultured samples. The bars show mean±SEM, n=6). *=p<0,05, **=p<0,01

<u>Supplemental Figure 1</u>: Negative controls of all immunohistochemical labelings. A) A1M-labeling. B) HO-1/Vimentin double labeling. C) GFAP labeling. D) NeuN labeling. E) Transducin labeling. Scale bar = 50μm.

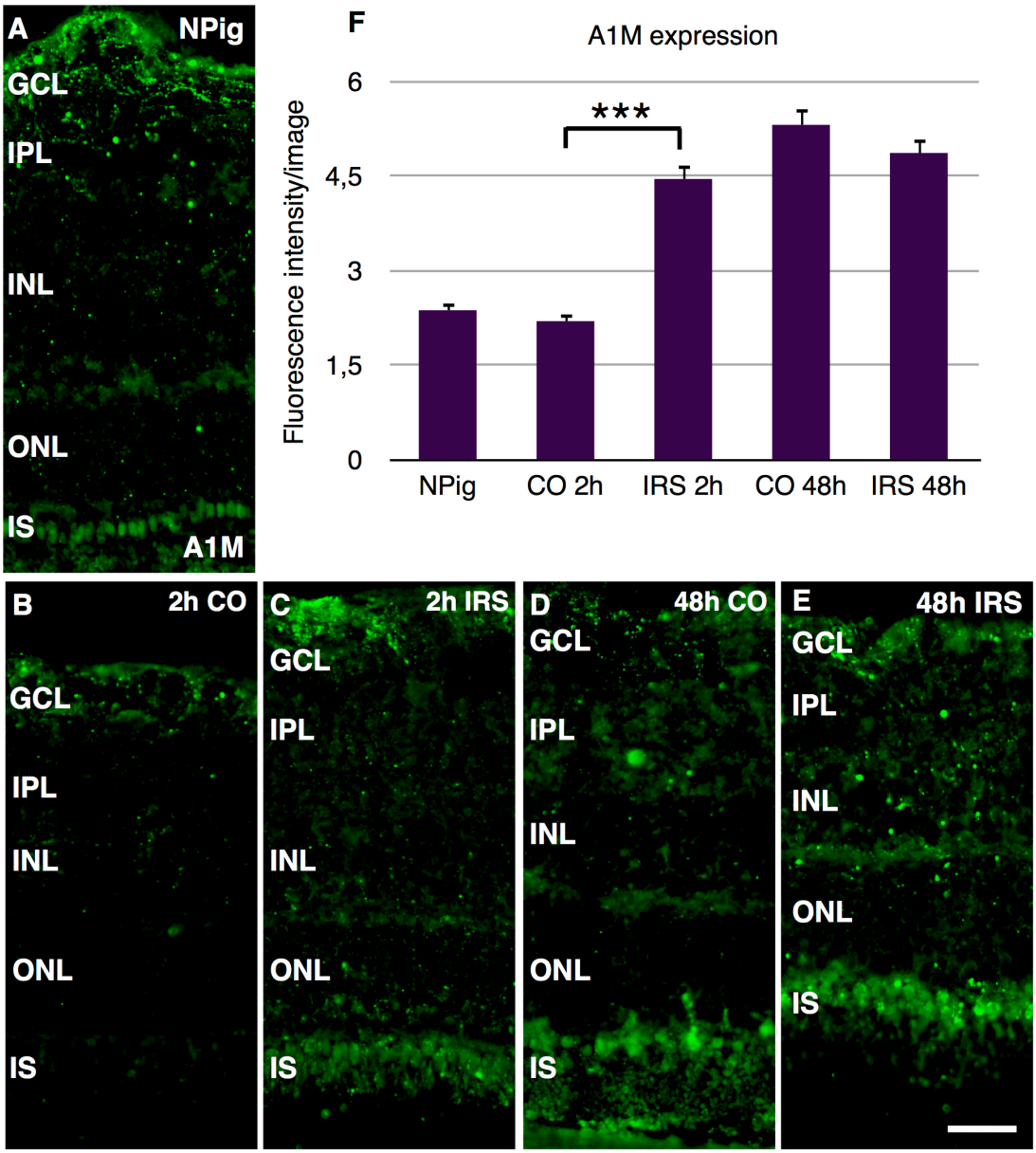
A
NPig
GCL
IPL
INL
ONL
IS
A1M
F
A1M expression
Fluorescence intensity/image
6
4,5
3
1,5
0
***
NPig
CO 2h
IRS 2h
CO 48h
IRS 48h
B
2h CO
C
2h IRS
D
48h CO
E
48h IRS

Figure 1.

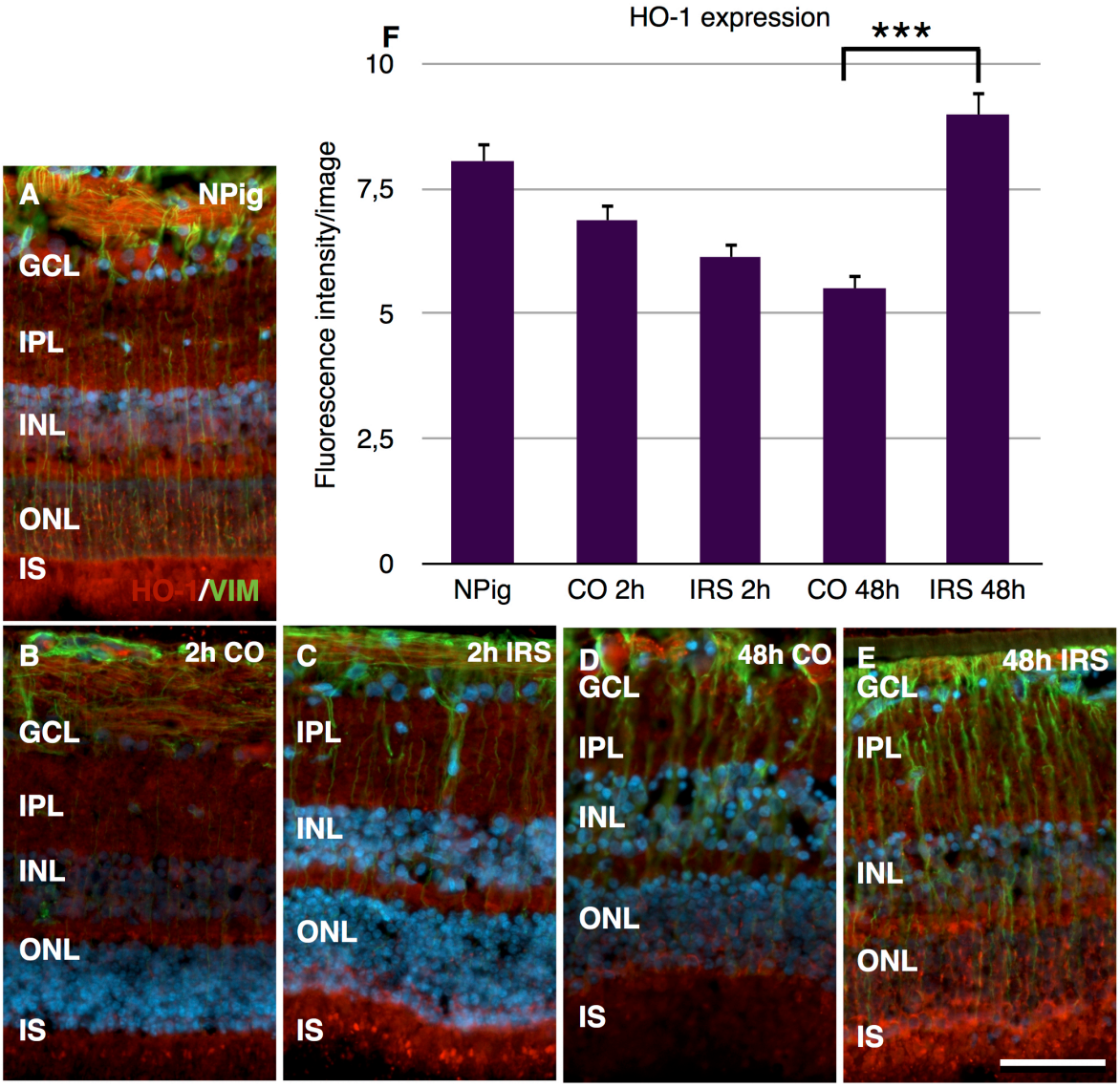
HO-1 expression
F
***
10
7,5
5
2,5
0
Fluorescence intensity/image
NPig
CO 2h
IRS 2h
CO 48h
IRS 48h
A
NPig
GCL
IPL
INL
ONL
IS
HO-1/VIM
B
2h CO
C
2h IRS
D
48h CO
E
48h IRS

Figure 2.

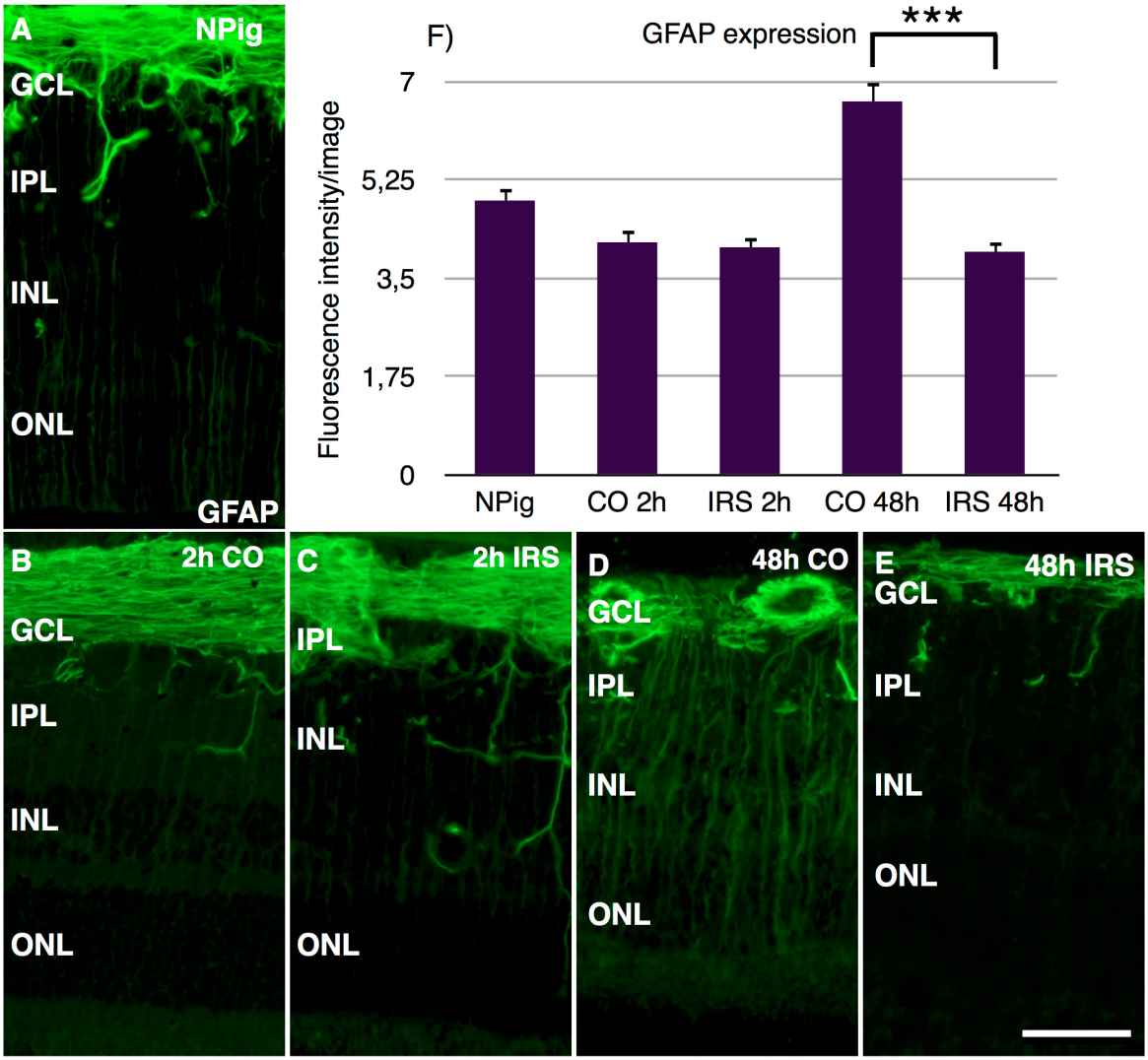
A
NPig
GCL
IPL
INL
ONL
GFAP
F)
GFAP expression
***
Fluorescence intensity/image
7
5,25
3,5
1,75
0
NPig
CO 2h
IRS 2h
CO 48h
IRS 48h
B
2h CO
C
2h IRS
D
48h CO
E
48h IRS

Figure 3.

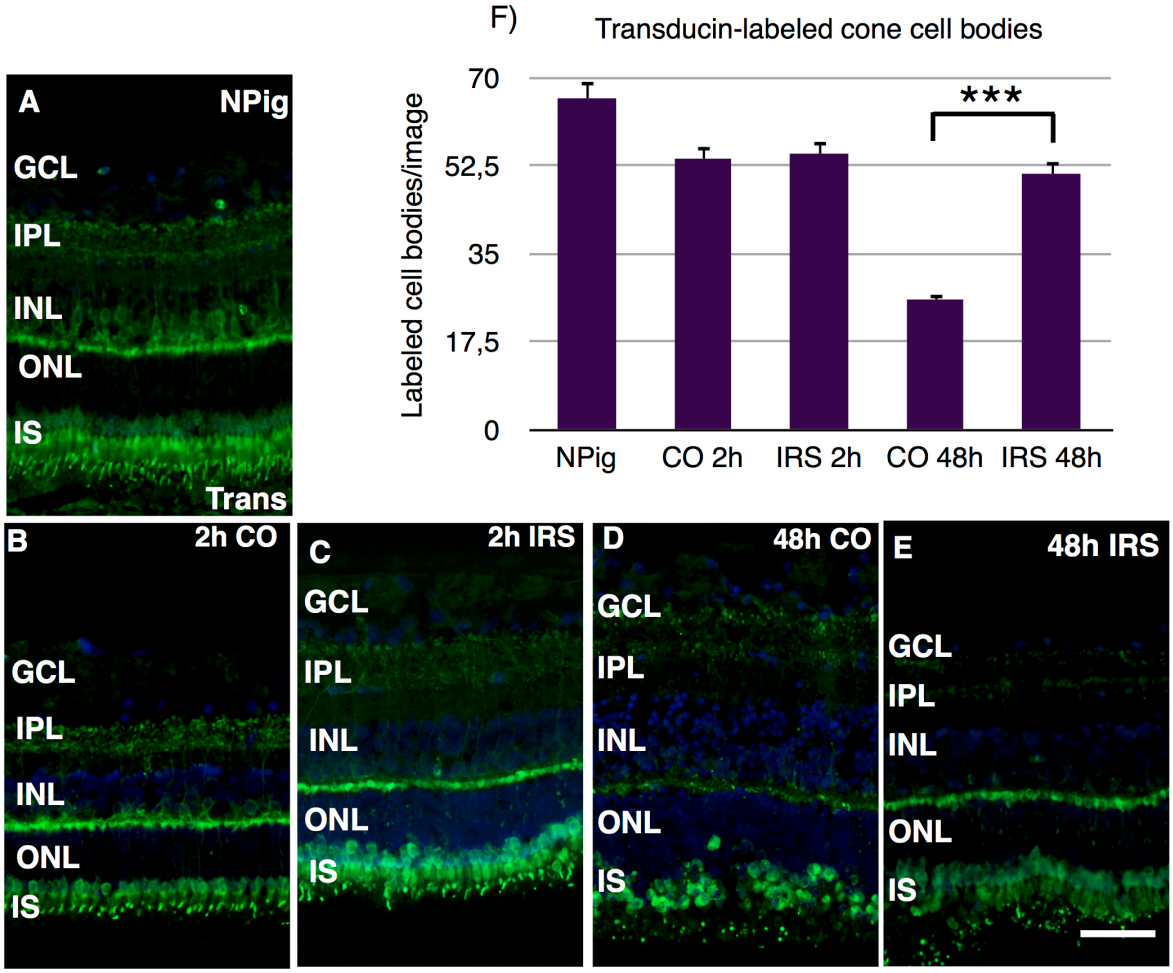
A
NPig
GCL
IPL
INL
ONL
IS
Trans
F)
Transducin-labeled cone cell bodies
Labeled cell bodies/image
70
52,5
35
17,5
0
***
NPig
CO 2h
IRS 2h
CO 48h
IRS 48h
B
2h CO
C
2h IRS
D
48h CO
E
48h IRS

Figure 4.

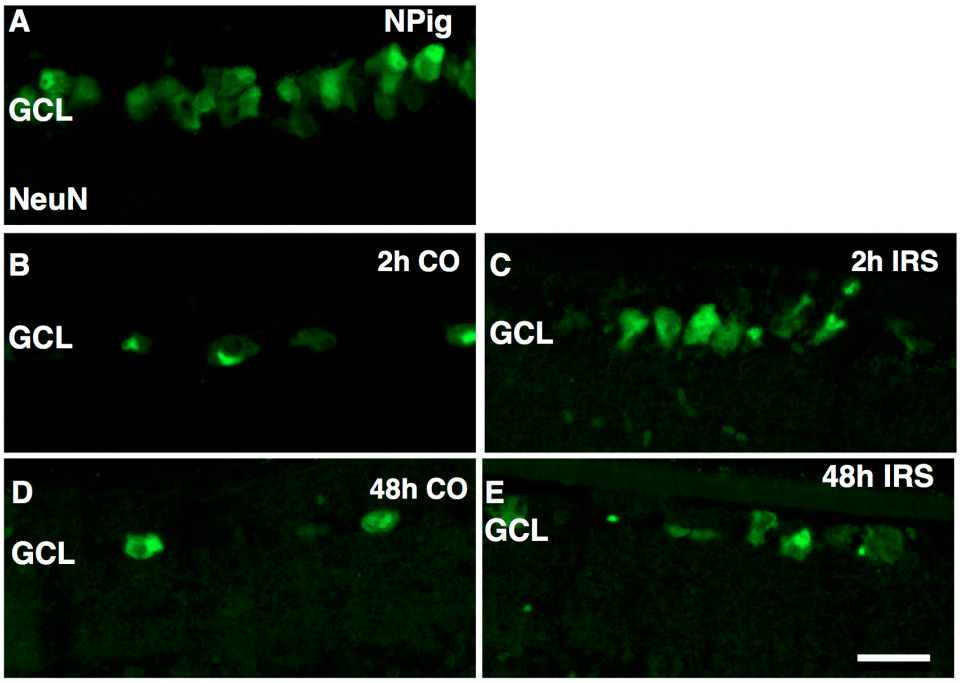
A
NPig
GCL
NeuN
B
2h CO
GCL
C
2h IRS
GCL
D
48h CO
GCL
E
48h IRS
GCL

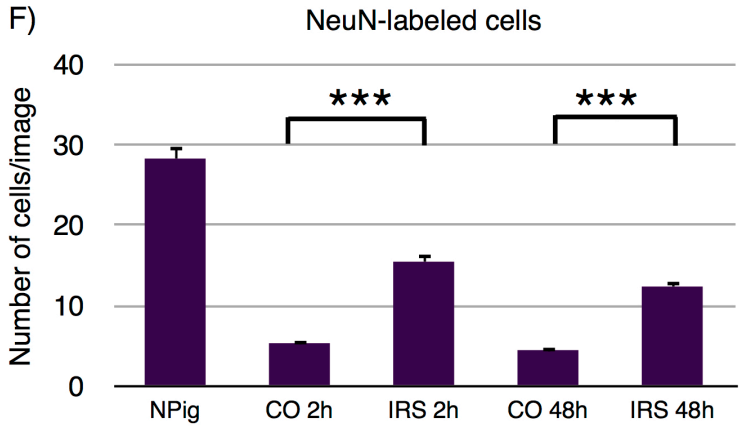
F)
NeuN-labeled cells
Number of cells/image
40
30
20
10
0
***
***
NPig
CO 2h
IRS 2h
CO 48h
IRS 48h

Figure 5.

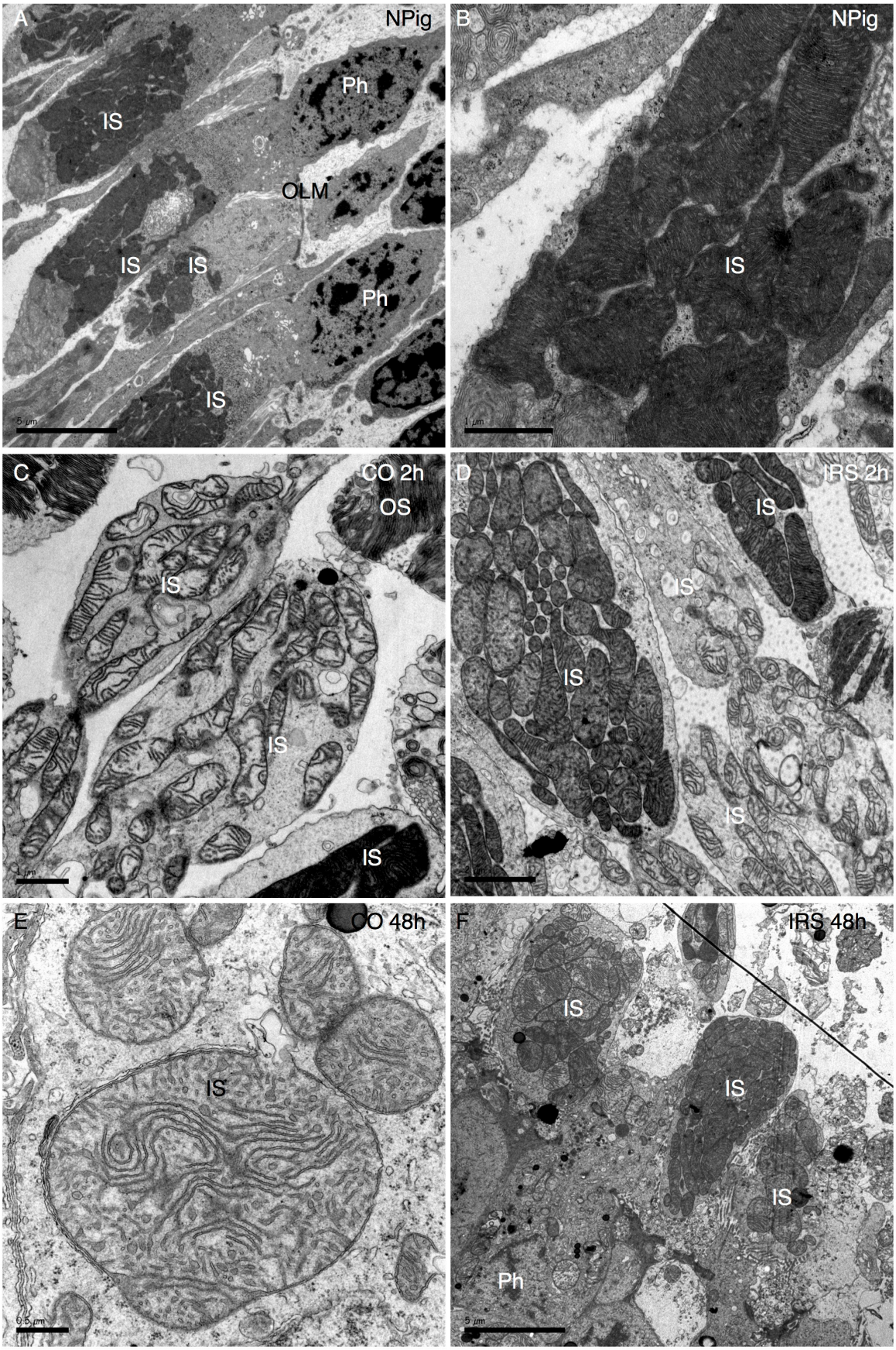
A
NPig
Ph
IS
OLM
IS
IS
Ph
IS
5 µm
B
NPig
IS
1 µm
C
CO 2h
OS
IS
IS
IS
1 µm
D
IRS 2h
IS
IS
IS
IS
E
CO 48h
IS
0,5 µm
F
IRS 48h
IS
IS
IS
Ph
5 µm

Figure 6.

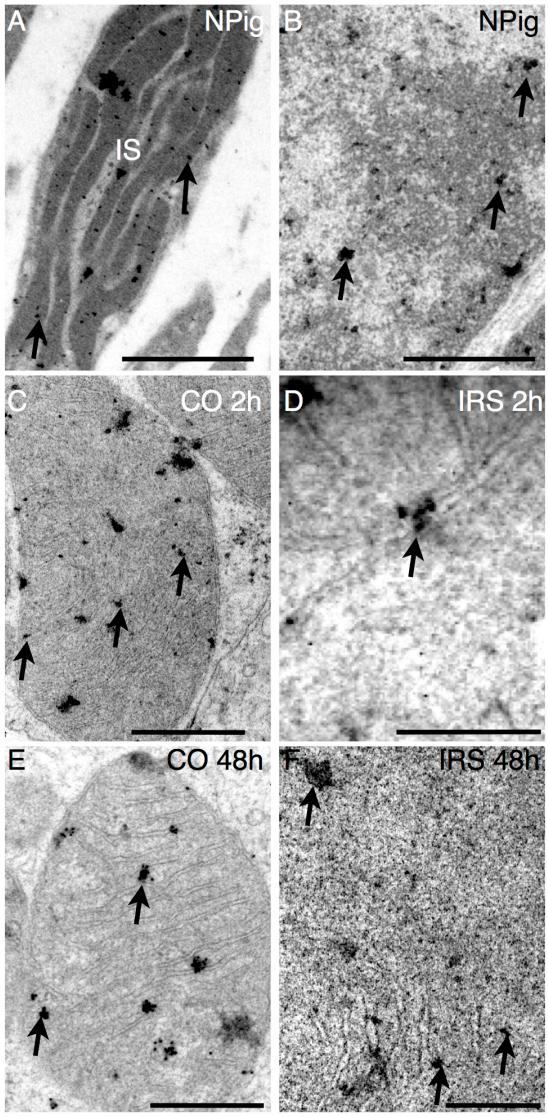

Figure 7.

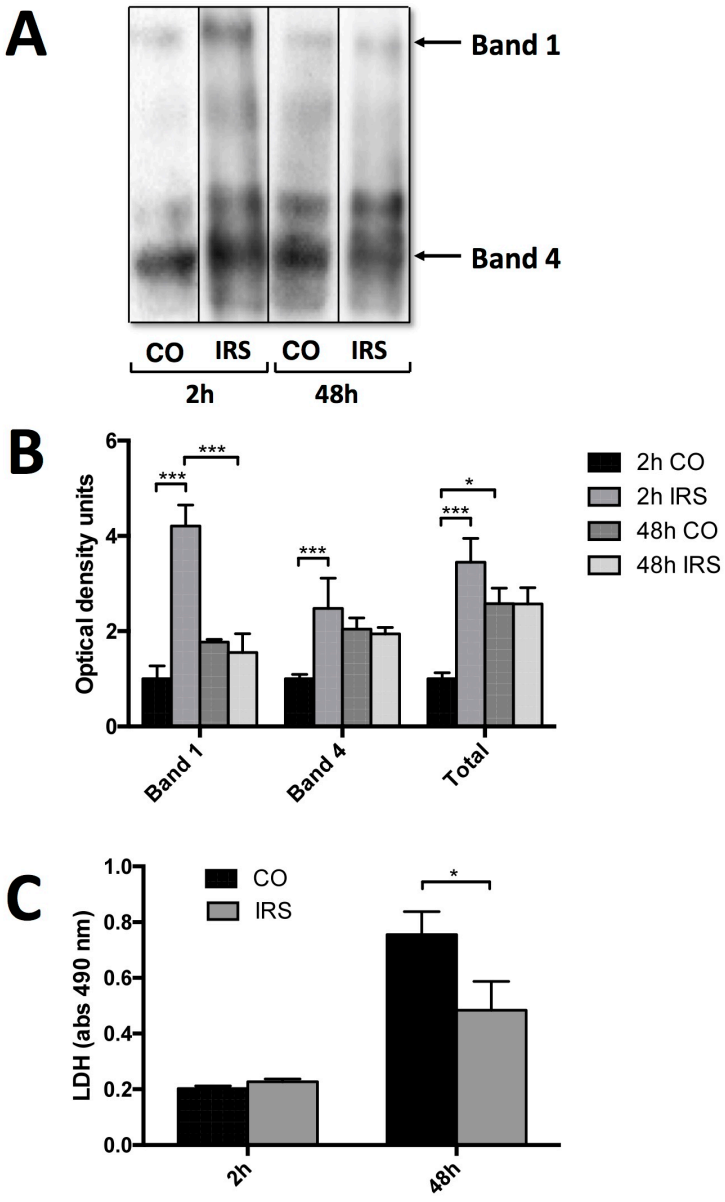
A
Band 1
Band 4
CO
IRS
CO
IRS
2h
48h
B
Optical density units
6
4
2
0
***
***
***
***
*
Band 1
Band 4
Total
2h CO
2h IRS
48h CO
48h IRS
C
LDH (abs 490 nm)
1.0
0.8
0.6
0.4
0.2
0.0
CO
IRS
*
2h
48h

Figure 8.

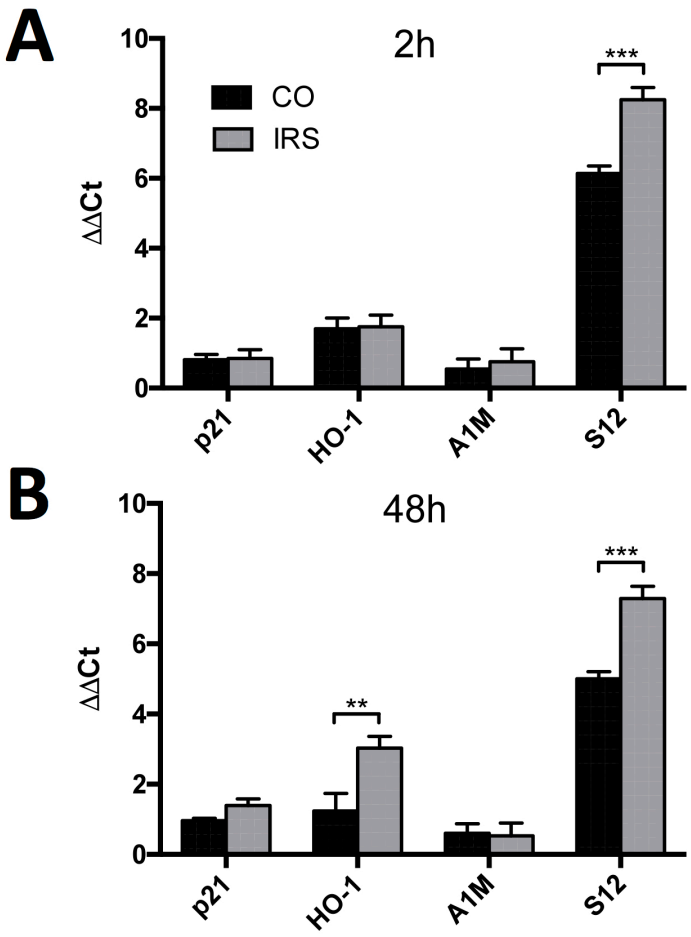
A
2h
CO
IRS
ΔΔCt
10
8
6
4
2
0
***
p21
HO-1
A1M
S12
B
48h
ΔΔCt
10
8
6
4
2
0
**
***
p21
HO-1
A1M
S12

Figure 9.

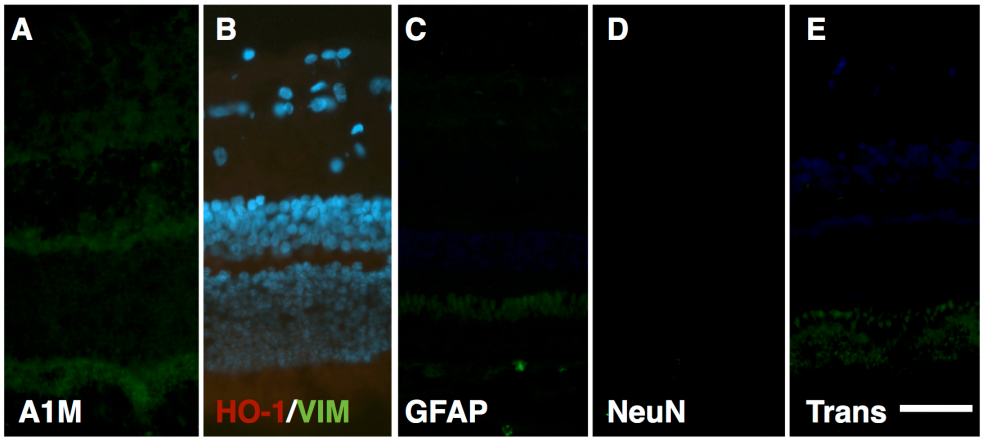

Supplemental figure 1.